IEEE Photonics Journal
An IEEE Photonics Society Publication

Open Access

Level Crossing Rate and Average Fade Duration of Satellite-to-UAV FSO Channels

Volume 13, Number 1, February 2021

Hoang D. Le, *Student Member, IEEE*
Anh T. Pham, *Senior Member, IEEE*

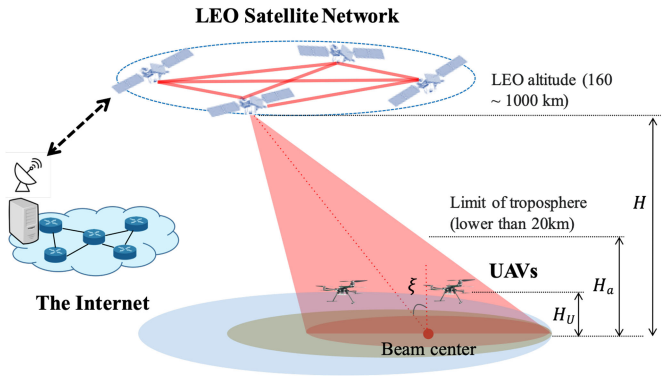

DOI: 10.1109/JPHOT.2021.3057198

Level Crossing Rate and Average Fade Duration of Satellite-to-UAV FSO Channels

Hoang D. Le, *Student Member, IEEE*, and Anh T. Pham, *Senior Member, IEEE*

Computer Communications Laboratory, The University of Aizu, Aizuwakamatsu 965-8580, Japan

DOI:10.1109/JPHOT.2021.3057198
This work is licensed under a Creative Commons Attribution 4.0 License. For more information, see https://creativecommons.org/licenses/by/4.0/

Manuscript received January 7, 2021; accepted February 1, 2021. Date of publication February 4, 2021; date of current version February 19, 2021. This work was supported in part by the University of Aizu's Competitive Fund under Grant number P5 and G33. The work of Hoang D. Le was supported by the Kubota fund. Corresponding author: Hoang D. Le (e-mail: hoangbkset@gmail.com).

Abstract: This paper investigates the second-order statistics of the level crossing rate (LCR) and average fade duration (AFD) for the optical wireless channels between a satellite and a vehicle. Specifically, the novel expressions of LCR and AFD for the low earth orbit (LEO) satellite-to-unmanned aerial vehicles (UAVs) laser links are derived in the presence of the generalized misalignments caused by the satellite vibration together with the UAV hovering, which is modeled by a four-parameter Beckmann distribution, and the atmospheric turbulence conditions. The analysis can also be applied to other kinds of vehicles, which, in fact, require simpler channel models. Several numerical examples are presented to quantitatively demonstrate the impact of both atmospheric turbulence and pointing errors on the LCR and AFD. The Monte Carlo simulations are performed to validate the correctness of the theoretical derivations.

Index Terms: Satellite-to-UAVs FSO link, generalized pointing error, level crossing rate, average fade duration.

1. Introduction

The ever-growing demand for reliable high-speed connections has become the major challenge for the design of the fifth-generation (5G) and beyond wireless communication networks [1]. Free space optical (FSO) communications, thanks to the capability to transport high-speed data over long distances without exhausting radio frequency (RF) resources, have been recently drawn a great deal of interest for wireless communication networks [2]. The FSO transmissions through the atmosphere, nevertheless, bring significant challenges. The uncertainty of atmospheric channels, especially the signal fading due to the atmospheric turbulence, together with the pointing errors caused by the random beam misalignments between transceivers pose various issues in the system design [3]. Studying statistical aspects of these adverse issues and understanding their impacts on the communication channels play an important role in the system design and performance optimization.

In the past few years, there have been many studies focusing on the analysis of first-order statistics of FSO channels, including the probability density function (PDF) and cumulative distribution function (CDF). These statistics can be used to obtain the static performance metrics

associated with FSO systems, such as outage probability, outage capacity, and bit error rate (BER) [4]. While the first-order statistics are essential in describing the overall distribution of fades in the turbulence fading channels, they nevertheless do not provide an indication of how these fades are distributed with respect to time. In order to describe the time-varying behavior of turbulence-induced fading channels, it is necessary to obtain its second-order statistics, such as the level crossing rate (LCR) and average fade duration (AFD) [5]. As a matter of fact, the LCR and AFD are especially essential in the cross-layer design and model of wireless communication systems, such as finite-state Markov modeling of turbulence fading channels [6], the estimation of packet error rates [7], the design of adaptive multi-rate systems over FSO turbulence links [8]. Furthermore, the second-order statistics are even more important than the first-order ones in some communication applications, such as adaptive transmission schemes, in which the average outage duration (AOD) is more critical than the probability of outage itself [9]. From the mathematical point of view, however, it is often difficult, if not impossible, to find the LCR and AFD of communication channels involving multiple random processes using a single composite random process followed by a direct application of the Rice formula [10].

Driven by the popularity of the FSO systems and the need to fully understand its time-varying behavior, a number of studies on second-order statistics of LCR and AFD for FSO terrestrial [11]–[14], inter-satellite [15], and satellite-to-ground links [16]–[18] have been reported. In particular, for the terrestrial FSO links, many of the prior studies focused on the investigation of the atmospheric turbulence, which has a significant effect on the system performance. Vetelino *et al.* analyzed the LCR over a range of turbulence conditions, i.e., from weak-to-strong, for the turbulence-induced fading channels modeled by the log-normal and Gamma-Gamma distributions [11]. In [12], the authors derived novel expressions of both LCR and AFD for the turbulence fading channels modeled by the generalized K-distribution. The LCR of Malaga $\mathcal{M}$-turbulent FSO links was reported in [13]. Most recently, the approximations of LCR and AOD for the terrestrial laser links in the presence of weak atmospheric turbulence modeled by the log-normal distribution and the Rice-induced pointing errors were derived in [14]. On the contrary, in the case of inter-satellite FSO links, the major challenge is the pointing errors due to the narrow laser beam pointing to/from moving platforms. For this reason, the authors in [15] investigated the LCR and AFD considering the random misalignments due to the vibration of satellites.

Regarding the FSO links between a satellite and ground stations, the existing studies mainly focused on the analysis of LCR and AFD in the presence of the atmospheric turbulence phenomenon for the uplink, i.e., the ground-to-satellite connections [17], [18]. It is worth noting that the issues involved in FSO uplink are different from that of a downlink in satellite communications. In the uplink, the laser beam immediately comes in contact with the atmospheric turbulence. Therefore, it suffers more severely from the distortion due to the spatial and temporal changes in the refractive index of the atmosphere. Meanwhile, the challenge in the downlink is primarily caused by the beam divergence loss, i.e., the geometric spreading loss and small spread due to the atmospheric turbulence. The effect of atmospheric turbulence is, therefore, generally small on the downlink propagation as the laser beam goes through a non-atmospheric path until it enters the troposphere, which is from the altitude of about 20 km to the ground level. The early effort studying the second-order statistics for the satellite-to-ground station laser links was reported by Andrews *et al.* [16], in which the LCR and AFD for the laser downlink from a satellite to a fixed ground station were investigated with the focus of the weak atmospheric turbulence conditions without the consideration of the pointing errors.

As the low-earth orbit (LEO) satellite-assisted communications have recently emerged for many applications ranging from fixed Internet access to autonomous, unmanned aerial vehicles (UAVs) for military missions, delivery services, and even temporary mobile base station (BS) [19], it becomes more crucial to understand the statistical behaviors of the satellite downlink channels when the ground station is a vehicle. Especially, in a particular case of a UAV in mobility, it is necessary to take into account the impact of channel misalignment due to the combined effects of satellite vibrations and UAV hovering. The second-order statistics of such channel, including LCR and AFD, to the best of our knowledge, is not available in the literature.

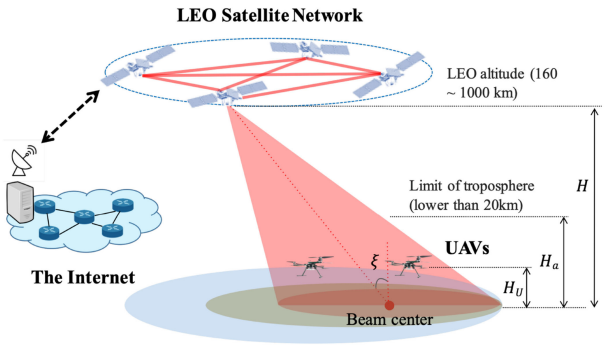

Fig. 1. Description of LEO satellite-based UAV network model.

In this paper, our aim is, therefore, to investigate and fully understand the second-order statistics of the laser links between a satellite and a vehicle. In particular, we derive the novel expressions for average LCR and AFD of LEO satellite-to-UAVs laser links in the presence of generalized misalignments due to the combined effect of satellite vibration and UAV hovering, which is modeled by a four-parameter Beckmann distribution, and the atmospheric turbulence conditions. Several numerical examples quantify the impacts of both atmospheric turbulence and pointing error on the average LCR and AFD. The Monte Carlo simulations are performed to validate the accuracy of theoretical derivations.

The remainder of the paper is organized as follows. The satellite-to-UAV channel models are presented in Section 2. In Section 3, we analyze and derive the novel expressions of the LCR and AFD for satellite-to-UAV laser links. Analytical and simulation results are given in Section 4. Finally, we conclude the paper in Section 5.

2. Satellite-to-UAV Channel Model

The LEO satellite-based UAV network model is described in Fig. 1, in which we consider the laser downlink from a satellite to UAVs in mobility. As multiple UAVs can be supported by a single laser beam, a UAV is not necessarily in the center of the laser beam footprint. In this section, we focus on investigating the main adverse issues on the FSO-based satellite-to-UAV channels, including the Doppler effect, atmospheric attenuation, atmospheric turbulence, and pointing error.

2.1 Doppler Effect

The Doppler effect is due to the relative motion between the LEO satellite and UAV, leading to the frequency shift of the received signals. Let f_c denote the center frequency of the transmitted laser signal, the Doppler frequency shift can be expressed as

$$\Delta f = -\frac{f_c\left(H_u+R_e\right)R_s\sin\left(\omega_F t\right)\sin\left(\cos^{-1}\left(\frac{H_u+R_e}{R_s}\sin\xi_{min}\right)+\xi_{min}\right)\omega_F}{c\sqrt{\left(H_u+R_e\right)^2+R_s^2-2\left(H_u+R_e\right)R_s\cos\left(\omega_F t\right)\sin\left(\cos^{-1}\left(\frac{H_u+R_e}{R_s}\sin\xi_{min}\right)+\xi_{min}\right)}}, \quad (1)$$

where c is the speed of light in vacuum, ξ_{min} is the minimum viewing zenith angle, ω_F is the relative angular velocity of the satellite with respect to UAV, R_s is the distance between the satellite and the center of the earth, while H_u and R_e are the UAV altitude and the radius of the earth, respectively [20]. As we assumed that the deployed UAVs hover at their own fixed positions, the velocity of UAV is approximately zero. As a result, the relative angular velocity, ω_F, can be determined based on the satellite velocity, i.e., $\omega_F = v_s/R_s$. Here, v_s is the LEO satellite velocity and can be computed as $v_s = \sqrt{\mu_G/R_s}$, where $\mu_G = 3.986 \times 10^{14}\text{m}^3/\text{s}^2$ is the gravitational constant times mass of earth [21].

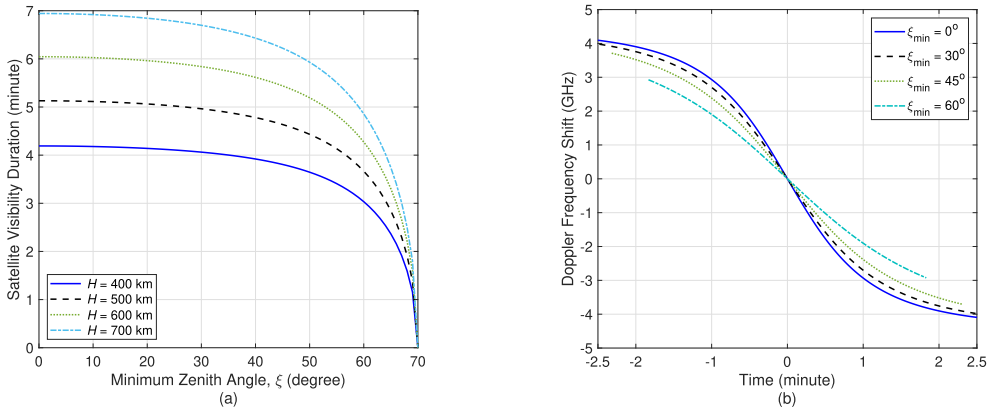

(a) (b)

Fig. 2. (a) Visibility duration within a satellite orbit, and (b) Doppler frequency shift with $H = 500$ km.

In addition, to investigate the Doppler effect with respect to time, it is essential to determine the satellite visibility window duration. It is defined as the total time that the LEO satellite can communicate effectively with the UAV within a small percentage of the satellite orbit period and can be written as

$$\tau\left(\xi_{\min}\right) \approx \frac{2}{\omega_{\mathrm{F}}} \cos^{-1}\left(\frac{\sin\left(\cos^{-1}\left(\frac{H_{\mathrm{u}}+R_{\mathrm{e}}}{R_{\mathrm{s}}}\sin\xi_{\max}\right)+\xi_{\max}\right)}{\sin\left(\cos^{-1}\left(\frac{H_{\mathrm{u}}+R_{\mathrm{e}}}{R_{\mathrm{s}}}\sin\xi_{\min}\right)+\xi_{\min}\right)}\right), \tag{2}$$

where $\xi_{\max}$ is the maximum viewing zenith angle for visibility [20]. As a matter of fact, in the presence of the Doppler effect, the bandwidth of receiver optical filter has to increase to receive the frequency-shifted optical signals, and thus leading to an extra background noise. An example of visibility duration within a satellite orbit and Doppler frequency shift are shown in Fig. 2(a) and 2(b), respectively, where $\xi_{\max} = 70^{\circ}$. In particular, as seen from Fig. 2(a), higher altitude of LEO satellite orbit, longer visibility duration is. In Fig. 2(b), the maximum Doppler frequency shift ranging from approximately -4 GHz to $+4$ GHz is observed at $\xi_{\min} = 0^{\circ}$. Such a maximum frequency shift is, nevertheless, within the capability of the current receiver design for the satellite laser communications, which is able to deal with the frequency shift up to ± 14 GHz [22]. As a result, the Doppler effect can be ignored in the analysis of the second-order statistic of FSO-based satellite links.

2.2 Atmospheric Attenuation

The atmospheric attenuation is caused by the molecular absorption and aerosol scattering suspended in the air, which can be described by the exponential Beer-Lambert's law as

$$h_{\mathrm{l}} = \exp(-\zeta L_{\mathrm{a}}), \tag{3}$$

where ζ is the attenuation coefficient [23]. The atmospheric attenuation mainly occurs in the troposphere, which an altitude of $H_{\mathrm{a}} \approx 20$ km and bellow. The propagation distance L_{a} therefore can be determined as $L_{\mathrm{a}} = (H_{\mathrm{a}} - H_{\mathrm{u}})\sec(\xi)$, where H_{u} is the UAV altitude. In addition, the attenuation coefficient ζ with the value of ζ_{dB} [dB/km] can be shown as

$$\zeta_{\mathrm{dB}} = \frac{3.91}{V[\mathrm{km}]}\left(\frac{\lambda[\mathrm{nm}]}{550}\right)^{-\varepsilon}, \tag{4}$$

where V is the visibility (i.e., the maximum distance that one object can be clearly discerned), λ is the optical wavelength while ε is the size distribution of the scattering particles and can be

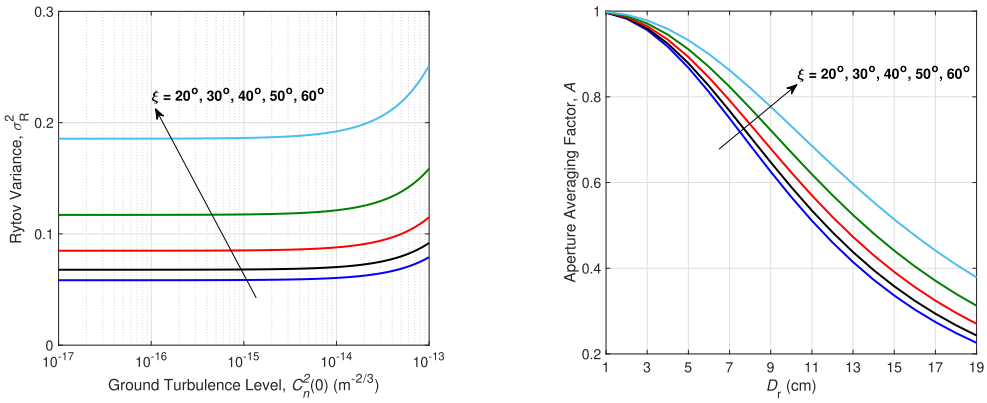

(a) (b)

Fig. 3. (a) Rytov variance, and (b) aperture averaging factor under different zenith angles.

determined by using Kim model [24], i.e.,

$$\varepsilon = \begin{cases} 1.6, & \text{if } V > 50\,\text{km}, \\ 1.3, & \text{if } 6\,\text{km} < V \leq 50\,\text{km}, \\ 0.16\,V + 0.34 & \text{if } 1\,\text{km} < V \leq 6\,\text{km}, \\ V - 0.5 & \text{if } 0.5\,\text{km} < V \leq 1\,\text{km}, \\ 0 & \text{if } V \leq 0.5\,\text{km}, \end{cases} \tag{5}$$

Here, the value of V depends on the weather conditions. For instance, $V > 50$ km when the weather is very clear sky, 1 km $< V \leq 6$ km for a hazy weather, and $V \leq 1$ km for a foggy condition [23]. Note that ζ in Eq. (3) is determined with $\zeta = \frac{\zeta_{\text{dB}}}{10^4 \log_{10} e}$ [m^{-1}].

2.3 Atmospheric Turbulence-Induced Fading

The atmospheric turbulence phenomenon causes the scintillation effect, which results in the received optical signal fluctuations at the UAV detector. In fact, the strength of turbulence is determined by the Rytov variance, denoted as σ_{R}^2, in which weak, moderate, and strong turbulence conditions correspond to $\sigma_{\text{R}}^2 < 1$, $\sigma_{\text{R}}^2 \approx 1$, and $\sigma_{\text{R}}^2 > 1$ [25]. For the LEO satellite-to-UAV optical links, the turbulence strength is usually weak in the case of small zenith angles as shown in Fig. 3(a). The intensity fluctuation probability density function (PDF), therefore, can be modeled as a log-normal distribution, in which the PDF of h_{a} is given by [19]

$$f_{h_{\text{a}}}(h_{\text{a}}) = \frac{1}{\sqrt{2\pi}\sigma_{\text{R}} h_{\text{a}}} \exp\left[-\frac{\left(\log(h_{\text{a}}) + \sigma_{\text{R}}^2/2\right)^2}{2\sigma_{\text{R}}^2} \right], \tag{6}$$

where σ_{R}^2 is the Rytov variance, and, in the case of plane wave propagation, it is given by

$$\sigma_{\text{R}}^2 = 2.25 k_{\text{wave}}^{7/6} \sec^{11/6}(\xi) \int_{H_{\text{u}}}^{H_{\text{a}}} C_n^2(h)\,(h - H_{\text{u}})^{5/6}\,dh, \tag{7}$$

where $k_{\text{wave}} = 2\pi/\lambda$ is the optical wave number corresponding to the optical wave length λ and ξ is the zenith angle [26]. Additionally, the variation of refractive index structure parameter, $C_n^2(h)$, according to altitude h can be expressed by the most widely used Hufnagel-Valley model, and is given by

$$C_n^2(h) = 0.00\,594 \left(\frac{v_{\text{wind}}}{27}\right)^2 (10^{-5}h)^{10} \exp\left(-\frac{h}{1000}\right)$$

$$+ 2.7 \times 10^{-16} \exp\left(-\frac{h}{1500}\right) + C_n^2(0) \exp\left(-\frac{h}{100}\right), \tag{8}$$

where $C_n^2(0)$ is the ground level turbulence varying from $10^{-17}\,\mathrm{m}^{-2/3}$ to $10^{-13}\,\mathrm{m}^{-2/3}$, and v_{wind} (m/s) is the root mean squared wind speed [26].

Another crucial issue to investigate is the aperture averaging effect, which illustrates the fact that an increase of receiver aperture size results in a decrease in power fluctuation level caused by the atmospheric turbulence. In other words, the receiver is able to average out the fluctuations over its large aperture, and the power fluctuations will be less than those from a point receiver. The aperture averaging factor, denoted by A, is defined as the ratio of the variation of the signal power fluctuations from a receiver with aperture diameter of D_{r} to that from a point receiver and can be written as

$$A = \frac{\sigma_I^2(D_{\mathrm{r}})}{\sigma_I^2(D_{\mathrm{r}}=0)} = \left[1 + 1.1\left(\frac{D_{\mathrm{r}}^2}{\lambda \Phi \sec(\xi)}\right)^{7/6}\right]^{-1}, \tag{9}$$

where σ_I^2 is the scintillation index, and in case of weak turbulence $\sigma_I^2 = \sigma_{\mathrm{R}}^2$ [3]. Here, it is noted that $\sigma_I^2(D_{\mathrm{r}}=0) = \sigma_{\mathrm{R}}^2$, in which σ_{R}^2 is shown in (7). In addition, H_{s} is the atmospheric turbulence aperture averaging scale height, which is given by [27]

$$\Phi = \left[\frac{\int_{H_{\mathrm{u}}}^{H_{\mathrm{a}}} C_n^2(h) h^2 dh}{\int_{H_{\mathrm{u}}}^{H_{\mathrm{a}}} C_n^2(h) h^{5/6} dh}\right]^{6/7}. \tag{10}$$

An example of aperture averaging effect with different values of receiver aperture diamter is depicted in Fig. 3(b). Also, $H = 500$ km, $H_{\mathrm{u}} = 100$ m, $C_n^2(0) = 10^{-14}\,\mathrm{m}^{-2/3}$, and different zenith angles are considered. As seen from the figure, UAV is considered as a point receiver when the aperture diameter is below 1 cm, and larger aperture diameter can mitigate the impact of atmospheric turbulence.

2.4 Generalized Pointing Error Model

The misalignment between the center of satellite beam footprint and that of UAV detector leads to the pointing errors and considerably degrades the system performance.[1] In our model, the misalignments illustrated in Fig. 4 are due to (i) the operation of UAV within a wide beam coverage of satellite at a distance of ρ, which is not necessarily at the center of beam footprint, (ii) the hovering of UAV around a certain position of UAV indicated by the displacement vector $\mathbf{r}_{\mathrm{U}} = (r_{\mathrm{U}_x}, r_{\mathrm{U}_y})$, in which r_{U_x} and r_{U_y} are modeled as independent zero-mean Gaussian random variables (RVs), i.e., $r_{\mathrm{U}_x} \sim \mathcal{N}(0, \sigma_{\mathrm{h}_x}^2)$ and $r_{\mathrm{U}_y} \sim \mathcal{N}(0, \sigma_{\mathrm{h}_y}^2)$, then the radial vector from this instantaneous position of UAV to the center of beam at P (in case of no vibration) can be expressed as $\mathbf{r}_{\mathrm{h}} = (r_{\mathrm{h}_x}, r_{\mathrm{h}_y})$ with $r_{\mathrm{h}_x} \sim \mathcal{N}(\rho_x, \sigma_{\mathrm{h}_x}^2)$ and $r_{\mathrm{h}_y} \sim \mathcal{N}(\rho_y, \sigma_{\mathrm{h}_y}^2)$, and (iii) the vibration of satellite beam footprint modeled by the radial vector $\mathbf{r}_s = (r_{\mathrm{s}_x}, r_{\mathrm{s}_y})$ from its initial position at P, where $r_{\mathrm{s}_x} \sim \mathcal{N}(0, \sigma_{\mathrm{s}_x}^2)$ and $r_{\mathrm{s}_y} \sim \mathcal{N}(0, \sigma_{\mathrm{s}_y}^2)$ and the values of $\sigma_{\mathrm{s}_x}, \sigma_{\mathrm{s}_y}$ can be expressed via the jitter angle θ_{jt}. Thus, the total radial displacement vector is expressed as $\mathbf{r} = \mathbf{r}_{\mathrm{h}} + \mathbf{r}_{\mathrm{s}}$ and its absolute value is shown as

$$\|\mathbf{r}\| = \sqrt{\|\mathbf{r}_{\mathrm{h}} + \mathbf{r}_{\mathrm{s}}\|^2} = \sqrt{r_{\mathrm{h}}^2 + 2\begin{bmatrix} r_{\mathrm{s}_x} \\ r_{\mathrm{s}_y} \end{bmatrix}^T \begin{bmatrix} r_{\mathrm{h}_x} \\ r_{\mathrm{h}_y} \end{bmatrix}^T + r_{\mathrm{s}}^2} = \sqrt{(r_{\mathrm{h}_x} + r_{\mathrm{s}_x})^2 + (r_{\mathrm{h}_y} + r_{\mathrm{s}_y})^2}, \tag{11}$$

where $\|\cdot\|$ is the norm of a vector, $[\cdot]^T$ is the transpose of a matrix, $r_x = r_{\mathrm{h}_x} + r_{\mathrm{s}_x} \sim \mathcal{N}(\rho_{\mathrm{x}}, \sigma_{\mathrm{h}_x}^2 + \sigma_{\mathrm{s}_x}^2)$ and $r_y = r_{\mathrm{h}_y} + r_{\mathrm{s}_y} \sim \mathcal{N}(\rho_{\mathrm{y}}, \sigma_{\mathrm{h}_y}^2 + \sigma_{\mathrm{s}_y}^2)$. In our case, the horizontal and vertical displacements of r, i.e.,

[1] The UAV detector can only capture a fraction of power from the satellite, which is known as the geometric loss. Moreover, when considering the Gaussian beam profile, the misalignment between the centers of UAV detector and satellite beam footprint further increases the geometric loss, which is so-called the misalignment loss.

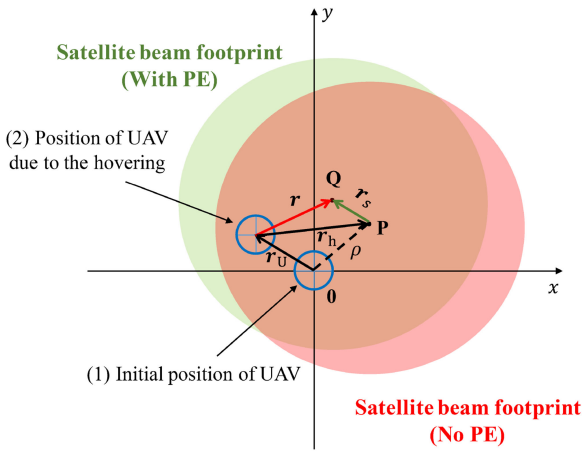

Fig. 4. Pointing errors due to the misalignment between UAV detector and satellite beam footprint center.

r_x and r_y, are two independent Gaussian RVs with different non-zero means $\{\rho_x, \rho_y\}$ and variances $\{\sigma_x^2, \sigma_y^2\}$, where $\sigma_x^2 \triangleq \sigma_{h_x}^2 + \sigma_{s_x}^2$ and $\sigma_y^2 \triangleq \sigma_{h_y}^2 + \sigma_{s_y}^2$, then r follows the Beckmann distribution with PDF given as [28]

$$f_r(r) = \frac{r}{2\pi\sigma_x\sigma_y}\int_0^{2\pi} \exp\left(-\frac{(r\cos\phi-\rho_x)^2}{2\sigma_x^2} - \frac{(r\sin\phi-\rho_y)^2}{2\sigma_y^2}\right) \mathrm{d}\phi. \tag{12}$$

The Beckmann distribution can be accurately approximated by a modified Rayleigh distribution, i.e.,

$$f_r(r) \simeq \frac{r}{\sigma_m^2}\exp\left(-\frac{r^2}{2\sigma_m^2}\right), r \geq 0, \tag{13}$$

where $\sigma_m^2 = (\frac{3\rho_x^2\sigma_x^4+3\rho_y^2\sigma_y^4+\sigma_x^6+\sigma_y^6}{2})^{1/3}$ is the approximated jitter variance [29].

On the other hand, considering a Gaussian beam footprint, the fraction of collected power of UAV (aperture radius of a) at the distance L due to the geometric spread with the radial displacement of r, can be approximated as

$$h_p \simeq A_0 \exp\left(-\frac{2r^2}{\omega_{L_{eq}}^2}\right), \tag{14}$$

where $A_0 = (\mathrm{erf}(\upsilon))^2$ is the fraction of the collected power at $r = 0$, $\mathrm{erf}(x) = \frac{2}{\sqrt{\pi}}\int_0^x \exp(-t^2)dt$ is the error function, $\upsilon = \frac{\sqrt{\pi}a}{\sqrt{2}\omega_L}$, $\omega_{L_{eq}}^2 = \omega_L^2 \frac{\sqrt{\pi}\mathrm{erf}(\upsilon)}{2\upsilon\exp(-\upsilon^2)}$ is the equivalent beam-width [28]. Here, ω_L is the effective beam-width at the distance L, given as $\omega_L = \omega_0\sqrt{(\Theta_0^2+\Lambda_0^2)(1+1.625\sigma_R^{12/5}\Lambda_1)}$, where σ_R^2 is the Rytov variance, $\omega_0 = \frac{2\lambda}{\pi\theta}$ is the beam waist at $L = 0$ with θ is the divergence angle, $\Theta_0 = 1 - \frac{L}{F_0}$ with F_0 is the radius of curvature, $\Lambda_0 = \frac{2L}{k_{wave}\omega_0^2}$ with k_{wave} is the optical wave number, and $\Lambda_1 = \frac{\Lambda_0}{\Theta_0^2+\Lambda_0^2}$ [24].

From (13) and (14), the PDF of h_p can be derived as

$$f_{h_p}(h_p) = \frac{\varphi_m^2}{h_p}\left(\frac{h_p}{A_m}\right)^{\varphi_m^2}, \ 0 \leq h_p \leq A_m, \tag{15}$$

where $A_m = A_0\exp(\frac{1}{\varphi_m^2} - \frac{1}{2\varphi_x^2} - \frac{1}{2\varphi_y^2} - \frac{\rho_x^2}{2\sigma_x^2\varphi_x^2} - \frac{\rho_y^2}{2\sigma_y^2\varphi_y^2})$, $\varphi_m = \frac{\omega_{L_{eq}}}{2\sigma_m}$, while $\varphi_x = \frac{\omega_{L_{eq}}}{2\sigma_x}$ and $\varphi_y = \frac{\omega_{L_{eq}}}{2\sigma_y}$ are the jitter variances in the x and y directions, respectively [29].

3. Second-Order Statistics

This section focuses on the expression derivation of level crossing rate (LCR) and average fade duration (AFD), which are the important metrics to describe the time-varying behavior of turbulence fading channels. In particular, the LCR and AFD are derived from the three factors, including atmospheric attenuation h_l, atmospheric turbulence h_a, pointing error h_p, which are assumed to be independent.[2] The composite channel coefficient, then, can be expressed as $h = h_\mathrm{l} h_\mathrm{a} h_\mathrm{p}$.

3.1 Level Crossing Rate

LCR is defined as the average number of upward (or downward) crossings per second at a given threshold h_0, and can be expressed as [5]

$$N_h(h_0) = \int_0^{+\infty} \dot{h} f_{h,\dot{h}}(h_0, \dot{h}) \mathrm{d}\dot{h}, \tag{16}$$

where $f_{h,\dot{h}}(\cdot,\cdot)$ is the joint PDF of h and its time derivative $\dot{h}$, which can be written as [32]

$$f_{h,\dot{h}}(h,\dot{h}) = \int_{\frac{h}{A_\mathrm{m} h_\mathrm{l}}}^{+\infty} \int_{-\infty}^{+\infty} \frac{1}{h_\mathrm{l}^2 h_\mathrm{a}^2} f_{h_\mathrm{p},\dot{h}_\mathrm{p}}\left(\frac{h}{h_\mathrm{l} h_\mathrm{a}}, \frac{\dot{h}}{h_\mathrm{l} h_\mathrm{a}} - \frac{\dot{h}_\mathrm{a} h}{h_\mathrm{l} h_\mathrm{a}^2}\right) f_{h_\mathrm{a},\dot{h}_\mathrm{a}}(h_\mathrm{a}, \dot{h}_\mathrm{a}) \mathrm{d}h_\mathrm{a} \mathrm{d}\dot{h}_\mathrm{a}, \tag{17}$$

where $f_{h_\mathrm{a},\dot{h}_\mathrm{a}}(\cdot,\cdot)$ is the joint PDF of h_a and its time derivative $\dot{h}_\mathrm{a}$, which can be expressed by

$$f_{h_\mathrm{a},\dot{h}_\mathrm{a}}(h_\mathrm{a},\dot{h}_\mathrm{a}) = \frac{1}{4\pi b \sigma_\mathrm{R} h_\mathrm{a}^2} \exp\left(-\frac{\dot{h}_\mathrm{a}^2}{8 b^2 h_\mathrm{a}^2}\right) \exp\left[-\frac{\left(\log(h_\mathrm{a}) + \sigma_\mathrm{R}^2/2\right)^2}{2\sigma_\mathrm{R}^2}\right], \tag{18}$$

where σ_R^2 is the Rytov variance [33]. Additionally, b is the standard deviation of the time derivative of a Gaussian random process and by applying the Taylor's frozen hypothesis of turbulence [34], it is given as $b = \frac{\sigma_\mathrm{R}}{\sqrt{2}\tau_0}$, where τ_0 is the channel coherence time, i.e., $\tau_0 = \frac{\sqrt{\lambda L}}{v_\mathrm{wind}}$ with λ is the wave length, L is the propagation distance, and v_wind is the rms wind speed.

On the other hand, to determine the joint PDF $f_{h_\mathrm{p},\dot{h}_\mathrm{p}}(\cdot,\cdot)$, we, first, need to find the joint PDF of the radial displacement r and its time derivative $\dot{r}$. In fact, the time derivative of r is independent from itself and follows the Gaussian PDF as in [5]. Then, from (13), the joint PDF of r and $\dot{r}$ can be given as

$$f_{r,\dot{r}}(r,\dot{r}) = \frac{r}{\sqrt{2\pi}\sigma_\mathrm{m}^2 \sigma_{\dot{r}}} \exp\left[-\left(\frac{r^2}{2\sigma_\mathrm{m}^2} + \frac{\dot{r}^2}{2\sigma_{\dot{r}}^2}\right)\right], \tag{19}$$

where σ_m^2 is given in (13), and $\sigma_{\dot{r}}^2$ is the variance of the time derivative of r. Here, $\sigma_{\dot{r}}$ can be calculated as $\sigma_{\dot{r}} = 2\pi f_0 \sigma_\mathrm{m}$, where $f_0 = f_\mathrm{s} + f_\mathrm{h}$ with f_s and f_h are the rms frequencies of satellite vibration and UAV hovering, respectively. In addition, from (14), r and $\dot{r}$ can be written as

$$r = \frac{\omega_{L_\mathrm{eq}}}{\sqrt{2}} \sqrt{\ln\left(\frac{A_0}{h_\mathrm{p}}\right)}, \quad \dot{r} = -\frac{\omega_{L_\mathrm{eq}} \dot{h}_\mathrm{p}}{2\sqrt{2} h_\mathrm{p} \sqrt{\ln\left(\frac{A_0}{h_\mathrm{p}}\right)}}, \tag{20}$$

where ω_{L_eq} and A_0 are defined in the pointing error model.

[2] It is worth noting that this assumption is widely accepted in the literature of FSO communications [4], [14], [23], [28], [30] As a matter of fact, in the clear sky conditions, the atmospheric attenuation is deterministic during a long time period [24], [31]. In addition, as the coherence time of atmospheric turbulence (10–100 ms) is much longer than that of satellite vibration (i.e., a few hundreds of microseconds [15]), the turbulence and pointing error can be considered to be independent.

From (19), (20), and by using the Jacobian of the transformation [35, Chap. 6], the joint PDF of $h_{\rm p}$ and $\dot{h}_{\rm p}$ can be derived as

$$f_{h_{\rm p},\dot{h}_{\rm p}}(h_{\rm p},\dot{h}_{\rm p})=\left|\begin{matrix}\frac{\partial r}{\partial h_{\rm p}} & \frac{\partial r}{\partial \dot{h}_{\rm p}}\\ \frac{\partial \dot{r}}{\partial h_{\rm p}} & \frac{\partial \dot{r}}{\partial \dot{h}_{\rm p}}\end{matrix}\right| f_{r,\dot{r}}(r,\dot{r})=\frac{\omega_{L_{\rm eq}}^2}{8h_{\rm p}^2\ln\left(\frac{A_0}{h_{\rm p}}\right)}f_{r,\dot{r}}(r,\dot{r})=\frac{\varphi_{\rm m}^3\left(\frac{A_0}{h_{\rm p}}\right)^{-\varphi_{\rm m}^2}\exp\left(-\frac{\varphi_{\rm m}^2\dot{h}_{\rm p}^2}{16\pi^2f_0^2h_{\rm p}^2\ln\left(\frac{A_0}{h_{\rm p}}\right)}\right)}{4\pi^{\frac{3}{2}}f_0h_{\rm p}^2\sqrt{\ln\left(\frac{A_0}{h_{\rm p}}\right)}},\tag{21}$$

where $\varphi_{\rm m}=\frac{\omega_{L_{\rm eq}}}{2\sigma_{\rm m}}$.

Plugging (18) and (21) into (17), the joint PDF of h and $\dot{h}$ can be expressed as

$$f_{h,\dot{h}}(h,\dot{h})=\int_{\frac{h}{A_{\rm m}h_{\rm l}}}^{+\infty}\int_{-\infty}^{+\infty}\frac{\varphi_{\rm m}^3\left(\frac{A_0h_{\rm l}h_{\rm a}}{h}\right)^{-\varphi_{\rm m}^2}}{16\pi^{\frac{5}{2}}f_0b\sigma_{\rm R}h^2h_{\rm a}^2\sqrt{\ln\left(\frac{A_0h_{\rm l}h_{\rm a}}{h}\right)}}\exp\left(-\frac{\dot{h}_{\rm a}^2}{8b^2h_{\rm a}^2}\right)\exp\left[-\frac{\varphi_{\rm m}^2\left(\frac{\dot{h}}{h}-\frac{\dot{h}_{\rm a}}{h_{\rm a}}\right)^2}{16\pi^2f_0^2\ln\left(\frac{A_0h_{\rm l}h_{\rm a}}{h}\right)}\right]$$
$$\times\exp\left[-\frac{\left(\log(h_{\rm a})+\sigma_{\rm R}^2/2\right)^2}{2\sigma_{\rm R}^2}\right]{\rm d}h_{\rm a}{\rm d}\dot{h}_{\rm a}.\tag{22}$$

To solve (22), we start the integral w.r.t of $\dot{h}_{\rm a}$, i.e.,

$$\int_{-\infty}^{+\infty}\exp\left(-\frac{\dot{h}_{\rm a}^2}{8b^2h_{\rm a}^2}\right)\exp\left[-\frac{\varphi_{\rm m}^2\left(\frac{\dot{h}}{h}-\frac{\dot{h}_{\rm a}}{h_{\rm a}}\right)^2}{16\pi^2f_0^2\ln\left(\frac{A_0h_{\rm l}h_{\rm a}}{h}\right)}\right]{\rm d}\dot{h}_{\rm a}$$
$$=\exp\left(-\frac{\varphi_{\rm m}^2\dot{h}^2}{16\pi^2f_0^2h^2\ln\left(\frac{A_0h_{\rm l}h_{\rm a}}{h}\right)}\right)\int_{-\infty}^{+\infty}\exp\left(-u\dot{h}_{\rm a}^2+2v\dot{h}_{\rm a}\right){\rm d}\dot{h}_{\rm a},\tag{23}$$

where $u=\frac{1}{8b^2h_{\rm a}^2}+\frac{\varphi_{\rm m}^2}{16\pi^2f_0^2h_{\rm a}^2\ln(\frac{A_0h_{\rm l}h_{\rm a}}{h})}$ and $v=\frac{\varphi_{\rm m}^2\dot{h}}{16\pi^2f_0^2hh_{\rm a}\ln(\frac{A_0h_{\rm l}h_{\rm a}}{h})}$. By using [36, (3.462.2)], the closed-form in (23) can be derived as

$$\int_{-\infty}^{+\infty}\exp\left(-\frac{\dot{h}_{\rm a}^2}{8b^2h_{\rm a}^2}\right)\exp\left[-\frac{\varphi_{\rm m}^2\left(\frac{\dot{h}}{h}-\frac{\dot{h}_{\rm a}}{h_{\rm a}}\right)^2}{16\pi^2f_0^2\ln\left(\frac{A_0h_{\rm l}h_{\rm a}}{h}\right)}\right]{\rm d}\dot{h}_{\rm a}$$
$$=\frac{8\sqrt{2}\pi^{\frac{3}{2}}f_0h_ab\sqrt{\ln\left(\frac{A_0h_{\rm l}h_{\rm a}}{h}\right)}}{\sqrt{16\pi^2f_0^2\ln\left(\frac{A_0h_{\rm l}h_{\rm a}}{h}\right)+8\varphi_{\rm m}^2b^2}}\exp\left[-\frac{\varphi_{\rm m}^2\dot{h}^2}{h^2\left(16\pi^2f_0^2\ln\left(\frac{A_0h_{\rm l}h_{\rm a}}{h}\right)+8\varphi_{\rm m}^2b^2\right)}\right].\tag{24}$$

Substituting (24) into (22) and making a change of variable, i.e., $y=\ln(\frac{A_0h_{\rm l}h_{\rm a}}{h})$, then

$$f_{h,\dot{h}}(h,\dot{h})=\frac{\varphi_{\rm m}^3}{\sqrt{2\pi}\sigma_{\rm R}h^2}\int_{\ln\left(\frac{A_0}{A_{\rm m}}\right)}^{+\infty}\frac{\exp\left(-\varphi_{\rm m}^2y-\frac{\left(y+\log\left(\frac{h}{A_0h_{\rm l}}\right)+\sigma_{\rm R}^2/2\right)^2}{2\sigma_{\rm R}^2}\right)}{\sqrt{16\pi^2f_0^2y+8\varphi_{\rm m}^2b^2}}\exp\left[-\frac{\varphi_{\rm m}^2\dot{h}^2}{h^2\left(16\pi^2f_0^2y+8\varphi_{\rm m}^2b^2\right)}\right]{\rm d}y.\tag{25}$$

Plugging (25) into (16), the LCR can be written as

$$N_h(h_0)=\frac{\varphi_{\rm m}^3}{\sqrt{2\pi}\sigma_{\rm R}h_0^2}\int_0^{+\infty}\int_{\ln\left(\frac{A_0}{A_{\rm m}}\right)}^{+\infty}\frac{\exp\left(-\varphi_{\rm m}^2y-\frac{\left(y+\log\left(\frac{h_0}{A_0h_{\rm l}}\right)+\sigma_{\rm R}^2/2\right)^2}{2\sigma_{\rm R}^2}\right)}{\sqrt{16\pi^2f_0^2y+8\varphi_{\rm m}^2b^2}}\dot{h}$$

$$\times \exp\left[-\frac{\varphi_{\mathrm{m}}^2 \dot{h}^2}{h_0^2\left(16\pi^2 f_0^2 y + 8\varphi_{\mathrm{m}}^2 b^2\right)}\right] \mathrm{d}\dot{h}\mathrm{d}y$$

$$= \frac{\varphi_{\mathrm{m}}}{\sqrt{\pi}\sigma_{\mathrm{R}}} \int_{\ln\left(\frac{A_0}{A_{\mathrm{m}}}\right)}^{+\infty} \sqrt{2\pi^2 f_0^2 y + \varphi_{\mathrm{m}}^2 b^2} \exp\left(-\varphi_{\mathrm{m}}^2 y - \frac{\left(y + \log\left(\frac{h_0}{A_0 h_{\mathrm{l}}}\right) + \sigma_{\mathrm{R}}^2/2\right)^2}{2\sigma_{\mathrm{R}}^2}\right) \mathrm{d}y. \tag{26}$$

By making the changes of variables along with some algebraic manipulations, the integral in (26) can be rewritten as

$$N_h(h_0) = \sqrt{\frac{2u}{\pi}}\varphi_{\mathrm{m}} \exp\left[\frac{\varphi_{\mathrm{m}}^2}{2}\left(\varphi_{\mathrm{m}}^2\sigma_{\mathrm{R}}^2 + 2\chi(h_0) - \frac{\sigma_{\mathrm{R}}\chi(h_0)\sqrt{u}}{\sqrt{2}\tau_0^2}\right)\right] \int_{X_0-\beta}^{+\infty} \sqrt{x+\beta}\exp\left(-ux^2\right)\mathrm{d}x, \tag{27}$$

where $u \triangleq \frac{1}{8\pi^4 f_0^4 \sigma_{\mathrm{R}}^2}$, $\chi(h_0) \triangleq \ln(\frac{h_0}{A_0 h_{\mathrm{l}}}) + 0.5\sigma_{\mathrm{R}}^2$, $\beta \triangleq \varphi_{\mathrm{m}}^2 b^2 - 2\pi^2 f_0^2(\varphi_{\mathrm{m}}^2\sigma_{\mathrm{R}}^2 + \chi(h_0))$, $X_0 \triangleq \varphi_{\mathrm{m}}^2 b^2 + 2\pi^2 f_0^2 \ln(\frac{A_0}{A_{\mathrm{m}}})$, and τ_0 is the channel coherence time. Using a series expansion of $\sqrt{x+\beta}$ in [37], [36, (1.111)] and an integral identity [36, (2.33.10)], i.e.,

$$\int x^m \exp\left(-\alpha x^n\right) dx = -\frac{\Gamma\left(\frac{m+1}{n}, \alpha x^n\right)}{n\alpha^{\frac{m+1}{n}}}, \sqrt{x+\beta} = \begin{cases} \sum_{k=0}^{+\infty}\binom{\frac{1}{2}}{k}\beta^k x^{\frac{1}{2}-k}, & \text{if } |x| \geq |\beta|, \\ \sum_{k=0}^{+\infty}\binom{\frac{1}{2}}{k}\beta^{\frac{1}{2}-k}x^k, & \text{if } |x| < |\beta|, \end{cases} \tag{28}$$

where $\Gamma(\alpha, x) = \int_x^{+\infty} \exp(-t)t^{\alpha-1}\mathrm{d}$ which is defined in [36, (8.350.2)], then we can get the infinite-series representation of LCR, which is shown as

$$N_h(h_0) = \sqrt{\frac{2u}{\pi}}\varphi_{\mathrm{m}} \exp\left[\frac{\varphi_{\mathrm{m}}^2}{2}\left(\varphi_{\mathrm{m}}^2\sigma_{\mathrm{R}}^2 + 2\chi(h_0) - \frac{\sigma_{\mathrm{R}}\chi(h_0)\sqrt{u}}{\sqrt{2}\tau_0^2}\right)\right]$$

$$\times \begin{cases} \sum_{k=0}^{+\infty} \frac{1}{2}\binom{\frac{1}{2}}{k} \frac{\beta^k}{u^{\frac{3-2k}{4}}}\Gamma\left(\frac{3-2k}{4}, u(X_0-\beta)^2\right), & \text{if } X_0 \geq 2\beta, \\ \sum_{k=0}^{+\infty} \frac{1}{2}\binom{\frac{1}{2}}{k}\left[\frac{\beta^k}{u^{\frac{3-2k}{4}}}\Gamma\left(\frac{3-2k}{4}, u\beta^2\right) + \frac{\beta^{\frac{1}{2}-k}}{u^{\frac{k+1}{2}}}\left(\Gamma\left(\frac{k+1}{2}, u(X_0-\beta)^2\right) - \Gamma\left(\frac{k+1}{2}, u\beta^2\right)\right)\right], & \text{if } X_0 < 2\beta. \end{cases} \tag{29}$$

Here, it is noted that (29) is convergent when the upper limit is large enough (i.e., about 50).

3.2 Average Fade Duration

AFD is defined as the average duration during which the signal stays below a given threshold of h_0, which is given as

$$T_h(h_0) = \frac{F_h(h_0)}{N_h(h_0)}, \tag{30}$$

where $N_h(h_0)$ is the level crossing rate [5]. In addition, $F_h(\cdot)$ is the cumulative distribution function (CDF) of h, which can be determined as

$$F_h(h_0) = \int_0^{h_0} f_h(h)\mathrm{d}h, \tag{31}$$

where $f_h(\cdot)$ is the composite PDF of $h = h_{\mathrm{l}}h_{\mathrm{a}}h_{\mathrm{p}}$ and from (3), (6), and (15), it can be computed as

$$f_h(h) = \int_0^{+\infty} f_{h|h_a}(h|h_a)f_{h_a}(h_a)dh_a = \int_{\frac{h}{A_{\mathrm{m}}h_{\mathrm{l}}}}^{+\infty} \frac{1}{h_a h_l} f_{h_p}\left(\frac{h}{h_a h_l}\right) f_{h_a}(h_a)\mathrm{d}h_a,$$

$$= \frac{\varphi_{\mathrm{m}}^2}{2\left(A_{\mathrm{m}}h_{\mathrm{l}}\right)^{\varphi_{\mathrm{m}}^2}} h^{\varphi_{\mathrm{m}}^2-1}\mathrm{erfc}\left(\frac{\ln\left(\frac{h}{A_{\mathrm{m}}h_{\mathrm{l}}}\right) + \mu}{\sqrt{2}\sigma_{\mathrm{R}}}\right)\exp\left(0.5\sigma_{\mathrm{R}}^2\varphi_{\mathrm{m}}^2\left(1+\varphi_{\mathrm{m}}^2\right)\right), \tag{32}$$

where $\mu = 0.5\sigma_R^2(1 + 2\varphi_m^2)$ and erfc(·) is the complementary error function [23]. Plugging (32) into (31), the CDF of h can be expressed as

$$F_h(h_0) = \frac{\varphi_m^2}{2\left(A_m h_l\right)^{\varphi_m^2}} \exp\left(0.5\sigma_R^2\varphi_m^2\left(1+\varphi_m^2\right)\right) \int_0^{h_0} h^{\varphi_m^2-1} \text{erfc}\left(\frac{\ln\left(\frac{h}{A_m h_l}\right)+\mu}{\sqrt{2}\sigma_R}\right) \text{d}h. \tag{33}$$

By making a change of variable, i.e., $z = \ln(\frac{h}{A_m h_l}) + \mu$ and using [37, (06.27.21.0011.01)], the closed-form in (33) can be derived as

$$F_h(h_0) = \frac{1}{2}\exp\left[\varphi_m^2\left(Z_0 - 0.5\sigma_R^2\varphi_m^2\right)\right]\text{erfc}\left(\frac{Z_0}{\sqrt{2}\sigma_R}\right) + \frac{1}{2}\text{erfc}\left(\frac{\sigma_R\varphi_m^2}{\sqrt{2}} - \frac{Z_0}{\sqrt{2}\sigma_R}\right), \tag{34}$$

where $Z_0 = \ln(\frac{h_0}{A_m h_l}) + \mu$.

4. Numerical Results and Discussions

In this section, we present several numerical examples of the LCR and AFD for the satellite-to-UAV laser links analyzed in Section 3 with different parameter settings. For the sake of convenience, given the crossing threshold h_0, we define the normalized fade level as

$$F_T = \frac{h_0}{\mathbb{E}(h)}, \tag{35}$$

where h is the composite channel coefficient, and $\mathbb{E}(\cdot)$ describes the average value. The parameters used in the analysis, unless otherwise noted, are as follows. Regarding the satellite: LEO satellite altitude $H = 500$ km, zenith angle $\xi = 50^o$, divergence angle $\theta = 223\,\mu$rad, optical wavelength $\lambda = 1.55\,\mu$m, phase front radius of laser beam $F_0 = 500$ m, and satellite vibration frequency $f_s = 100$ Hz. Additionally, the considered satellite vibration jitter angles are 6.69 μrad, 8.92 μrad, 11.15 μrad, and 15.61 μrad representing for 3%, 4%, 5%, and 7% of satellite divergence angle, respectively. For the parameters related to UAVs, UAV altitude $H_u = 100$ m, aperture diameter $D_r = 10$ cm, the initial position $\rho = 0$ m, the hovering jitter variances $(\sigma_{h_x}^2, \sigma_{h_y}^2) = (0.8$ m, 1 m), the frequency of hovering $f_h = 0$ Hz. As for the atmospheric turbulence, ground turbulence level $C_n^2(0) = 1.7 \times 10^{-14}\,\text{m}^{-2/3}$, atmospheric altitude $H_a = 20$ km, wind speed $v_{\text{wind}} = 21$ m/s, visibility (clear sky) $V = 20$ km. The Monte-Carlo simulations using the MATLAB programming are also provided to validate the analytical results.

First, we investigate the average LCR and AFD at the different normalized fade levels illustrated in Fig. 5(a) and 5(b), respectively. Also, different satellite vibration jitter angles and UAV's initial positions are considered. It is evident from Fig. 5(a) that the average LCR increases with an increase of the normalized fade level F_T and after reaching a maximum value, it decrease. In addition, it is observed in Fig. 5(b) that the AFD becomes longer with a higher value of F_T. In fact, for example, the level for the outage is set to $F_T = -3$ dB, then the AFD of this level is so-called average outage duration (AOD), which is an important parameter for system performance evaluation. For instance, at this outage level, i.e., $F_T = -3$ dB, the AOD is about a few milliseconds depending on the values of vibration jitter angle and UAV's initial position. Also in these figures, the analytical results follow the simulated ones very closely, which confirms the correctness of the analysis. For the next discussions, we consider $F_T = -3$ dB as the outage threshold of the considered system. Next, we analyze in Fig. 6 the average LCR and AFD in terms of zenith angles over a range of satellite vibration jitter angles, when $F_T = -3$ dB. There are two remarkable observations here. *First*, as can be seen in Fig. 6(a), an increase of zenith angle results in an increase of the average LCR due to the fact that the received signal fluctuates more frequently around the considered fade level. In addition, a longer AFD is observed at a higher value of zenith angle. The reason is that the fluctuation of signal tends to be at the lower fade levels at the large zenith angles. Indeed, at a low fade level, e.g., $F_T = -3$ dB in this particular case, the observation of AFD plays an essential role in the system performance evaluation, in which a longer AFD at this fade level leads to the

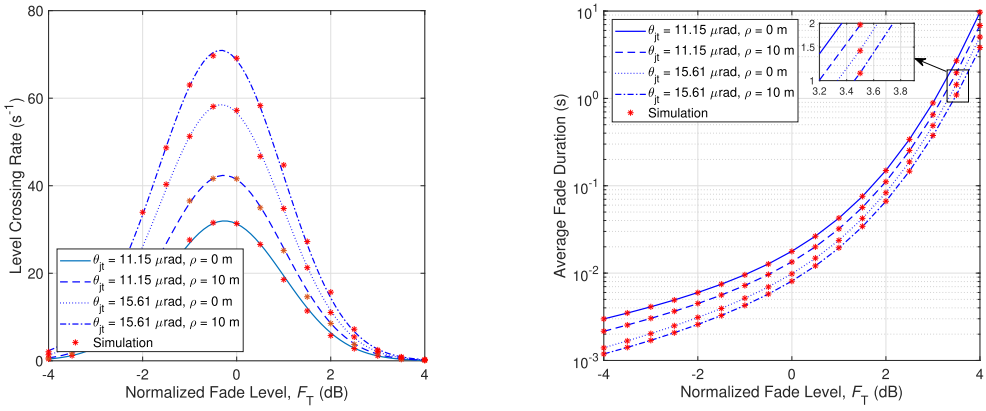

(a) (b)

Fig. 5. (a) Average LCR, and (b) AFD versus normalized fade level for different pointing error conditions.

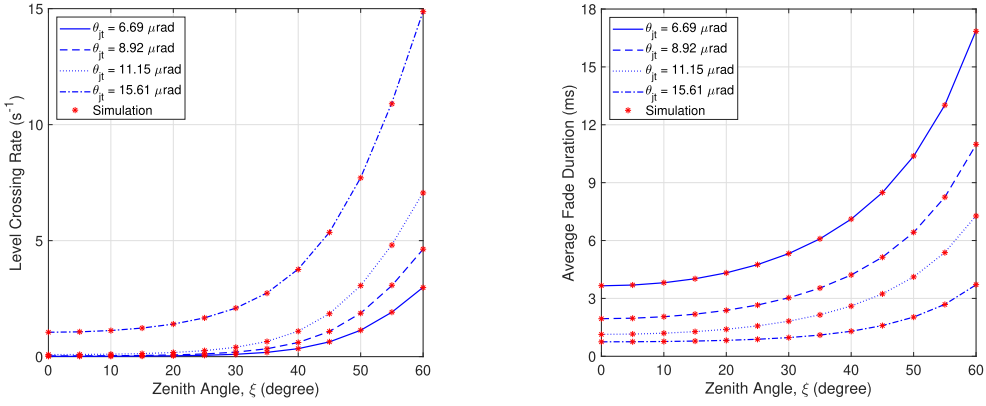

(a) (b)

Fig. 6. (a) Average LCR, and (b) AFD versus satellite zenith angle for different pointing error conditions.

significant degradation of system performance and the performance improvement methods need to be addressed. For example, when $\theta_{jt} = 11.15\,\mu$rad, the AFDs are from 1 ms and 7 ms as the zenith angle varies between $\xi = 0^o$ and $\xi = 60^o$. *Second*, the severity of pointing error indicated by the satellite vibration jitter angle has a significant impact on both average LCR and AFD as shown in the corresponding Figs. 6(a) and 6(b). For instance, when $\xi = 60^o$ and the satellite vibration angle varies from $\theta_{jt} = 6.69\,\mu$rad to $\theta_{jt} = 15.61\,\mu$rad, the average LCR increases from 3 s^{-1} to 15 s^{-1}, while a shorter AFD is observed that decreases from 17 ms to 4 ms, as illustrated in Fig. 6.

Finally, we examine the combined impact of atmospheric turbulence and pointing error on the LCR and AFD in Fig. 7, when $F_T = -3$ dB and $\theta_{jt} = 11.15\,\mu$rad. Also, different values of UAV aperture diameter and its initial position compared to the beam center are considered. As seen in Fig. 7(a), the severe pointing errors combined with the atmospheric turbulence significantly increase the average LCR. For example, when $D_r = 5$ cm, the average LCR increases from 5 s^{-1} to 9 s^{-1} as the combined pointing error and atmospheric turbulence vary from $\rho = 0$ m, $C_n^2(0) = 10^{-15}\,\text{m}^{-2/3}$ to $\rho = 10$ m, $C_n^2(0) = 10^{-13}\,\text{m}^{-2/3}$. In addition, a longer AFD is observed as the turbulence strength increases in Fig. 7(b). At a certain turbulence strength level, the signals fluctuate more often as the pointing error is more severe, resulting in a decrease of AFD at the considered fade level. For instance, when $D_r = 5$ cm and $\rho = 5$ m, the AFD increases from 5 ms to 6.1 ms as turbulence strengths are between $C_n^2(0) = 10^{-15}\,\text{m}^{-2/3}$ and $C_n^2(0) = 10^{-13}\,\text{m}^{-2/3}$. At

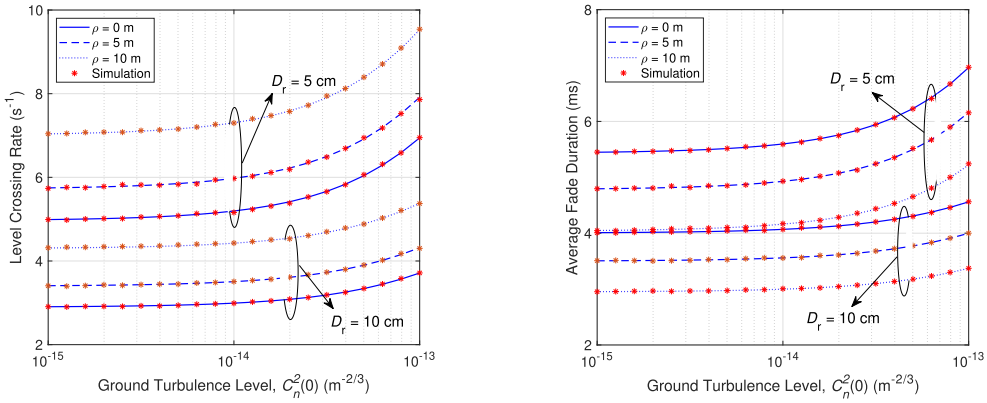

Fig. 7. (a) Average LCR, and (b) AFD for different turbulence conditions and UAV's initial positions.

$C_n^2(0) = 10^{-13}\,\mathrm{m}^{-2/3}$ and $D_\mathrm{r} = 5$ cm, the AFD decreases from 7 ms to 5 ms, when the pointing error is more severe represented by the increase from $\rho = 0\,\mathrm{m}$ to $\rho = 10\,\mathrm{m}$. On the other hand, using this figure, we highlight the effectiveness of aperture averaging effect, in which an increase of aperture diameter results in a decrease of LCR and AFD at the low fade levels.

5. Conclusion

In this paper, we have investigated the second-order statistics of satellite-to-UAV FSO links. The novel expressions of two important second-order statistics, i.e., LCR and AFD, were derived considering the generalized misalignments due to the combined effect of satellite vibration and UAV hovering, which was modeled by a four-parameter Beckmann distribution, and the atmospheric turbulence conditions. The analysis can be also applied to other kinds of vehicles, which, in fact, require simpler channel models. Numerical results were presented to illustrate some examples of LCR and AFD and showed that the severity of both atmospheric turbulence and pointing error has a significant impact on the LCR and AFD. The Monte Carlo simulations were performed to validate the theoretical analysis and the excellent agreements between the analytical and simulation results were confirmed.

Acknowledgment

The authors would like to thank anonymous reviewers for their constructive comments and useful suggestions, which help us a lot in improving the quality of the paper. The authors also would like to acknowledge Dr. Thanh V. Pham for his helpful advice on mathematical problems in this paper.

References

[1] K. Samdanis and T. Taleb, "The road beyond 5G: A vision and insight of the key technologies," *IEEE Netw.*, vol. 34, no. 2, pp. 135–141, Feb. 2020.
[2] A. S. Hamza, J. S. Deogun, and D. R. Alexander, "Classification framework for free space optical communication links and systems," *IEEE Commun. Surveys Tuts.*, vol. 21, no. 2, pp. 1346–1382, Oct. 2019.
[3] H. Kaushal and G. Kaddoum, "Optical communication in space: Challenges and mitigation techniques," *IEEE Commun. Surveys Tuts.*, vol. 19, no. 1, pp. 57–96, Jan. 2017.
[4] F. Yang, J. Cheng, and T. A. Tsiftsis, "Free-space optical communication with nonzero boresight pointing errors," *IEEE Trans. Commun.*, vol. 62, no. 2, pp. 713–725, Feb. 2014.
[5] Z. Hadzi-Velkov, N. Zlatanov, and G. K. Karagiannidis, "Level crossing rate and average fade duration of the multihop Rayleigh fading channel," in *Proc. IEEE Int. Conf. Commun.*, 2008, pp. 4451–4455.
[6] V. V. Mai and A. T. Pham, "Cross-layer designs and analysis of adaptive-rate transmission and ARQ for free-space optical communications," *IEEE Photon. J.*, vol. 8, no. 1, Jan. 2016, Art. no. 7901015.

[7] A. O. D. Ali, C. M. Yetis, and M. Torlak, "Novel expressions and applications for the level crossing rate of maximal ratio combining in the presence of cochannel interferers," *IEEE Trans. Veh. Technol.*, vol. 66, no. 11, pp. 9793–9808, Jun. 2017.
[8] H. D. Le, V. V. Mai, C. T. Nguyen, and A. T. Pham, "Design and analysis of sliding window arq protocols with rate adaptation for burst transmission over fso turbulence channels," *IEEE/OSA J. Opt. Commun. Netw.*, vol. 11, no. 5, pp. 151–163, May 2019.
[9] L. Yang and M. Alouini, "On the average outage rate and average outage duration of wireless communication systems with multiple cochannel interferers," *IEEE Trans. Wireless Commun.*, vol. 3, no. 4, pp. 1142–1153, Jul. 2004.
[10] L. Yang and M. Alouini, "Level crossing rate over multiple independent random processes: An extension of the applicability of the rice formula," *IEEE Trans. Wireless Commun.*, vol. 6, no. 12, pp. 4280–4284, Dec. 2007.
[11] F. S. Vetelino, C. Young, and L. Andrews, "Fade statistics and aperture averaging for gaussian beam waves in moderate-to-strong turbulence," *OSA Appl. Opt.*, vol. 46, no. 18, pp. 3780–3789, Jun. 2007.
[12] K. Yiannopoulos, N. C. Sagias, and A. C. Boucouvalas, "On the performance of semiconductor optical amplifier-assisted outdoor optical wireless links," *IEEE J. Sel. Areas Commun.*, vol. 33, no. 9, pp. 1869–1876, Sep. 2015.
[13] J. M. C. V. J. Navas and A. G. Balsells, "Fade statistics of M-turbulent optical links," *EURASIP J. Wireless Com. Netw.*, vol. 17, no. 1, pp. 1687–1499, Jun. 2017.
[14] C. B. Issaid and M. Alouini, "Level crossing rate and average outage duration of free space optical links," *IEEE Trans. Commun.*, vol. 67, no. 9, pp. 6234–6242, Sep. 2019.
[15] R. R. Hayes, "Fading statistics for intersatellite optical communication," *OSA Appl. Opt.*, vol. 36, no. 30, pp. 8063–8068, Oct. 1997.
[16] L. C. Andrews, R. L. Phillips, and P. T. Yu, "Optical scintillations and fade statistics for a satellite-communication system," *OSA Appl. Opt.*, vol. 34, no. 33, pp. 2875–2885, Nov. 1995.
[17] S. Basu, D. Voelz, and D. K. Borah, "Fade statistics of a ground-to-satellite optical link in the presence of lead-ahead and aperture mismatch," *OSA Appl. Opt.*, vol. 48, no. 7, pp. 1274–1287, Mar. 2009.
[18] H. T. Yura and R. A. Fields, "Level crossing statistics for optical beam wander in a turbulent atmosphere with applications to ground-to-space laser communications," *OSA Appl. Opt.*, vol. 50, no. 18, pp. 2875–2885, Jun. 2011.
[19] M. Li, Y. Hong, C. Zeng, Y. Song, and X. Zhang, "Investigation on the UAV-to-satellite optical communication systems," *IEEE J. Sel. Areas Commun.*, vol. 36, no. 9, pp. 2128–2138, Aug. 2018.
[20] I. Ali, N. Al-Dhahir, and J. E. Hershey, "Doppler characterization for satellites," *IEEE Trans. Commun.*, vol. 46, no. 3, pp. 309–313, Mar. 1998.
[21] Y. Shoji, M. J. Fice, Y. Takayama, and A. J. Seeds, "A pilot-carrier coherent-to-ground downlink system using an optical injection phase lock loop technique," *J. Lightw. Technol.*, vol. 30, no. 16, pp. 2696–2706, Jun. 2012.
[22] J. Li *et al.*, "Broadband laser doppler frequency shift emulator for satellite laser communication," *IEEE Photon. J.*, vol. 11, no. 6, Nov. 2019, Art. no. 5503612.
[23] M. T. Dabiri, S. M. S. Sadough, and I. S. Ansari, "Tractable optical channel modeling between UAVs," *IEEE Trans. Veh. Technol.*, vol. 68, no. 12, pp. 11543–11550, Dec. 2019.
[24] L. C. Andrews and R. L. Phillips, *Laser Beam Propagation Through Random Media*. Bellingham, WA, USA: SPIE Press, 2nd ed., 2005.
[25] H. Safi, A. A. Sharifi, M. T. Dabiri, I. S. Ansari, and J. Cheng, "Adaptive channel coding and power control for practical fso communication systems under channel estimation error," *IEEE Trans. Veh. Technol.*, vol. 68, no. 8, pp. 7566–7577, Aug. 2019.
[26] D. R. Kolev and M. Toyoshima, "Received-power fluctuation analysis for satellite-to-ground laser links," *J. Lightw. Technol.*, vol. 35, no. 1, pp. 103–112, Nov. 2017.
[27] A. Kumar and V. K. Jain, "Antenna aperture averaging with different modulation schemes for optical satellite communication links," *OSA J. Opt. Netw.*, vol. 6, no. 12, pp. 1323–1328, Dec. 2007.
[28] H. AlQuwaiee, H. Yang, and M. Alouini, "On the asymptotic capacity of dual-aperture systems with generalized pointing error model," *IEEE Trans. Wireless Commun.*, vol. 15, no. 9, pp. 6502–6512, Jun. 2016.
[29] R. Boluda-Ruiz, A. Garcia-Zambrana, C. Castillo-Vazquez, and B. Castillo-Vazquez, "Novel approximation of misalignment fading modeled by beckmann distribution on free-space optical links," *OSA Opt. Exp.*, vol. 24, no. 20, pp. 22635–22649, Oct. 2016.
[30] E. Zedini, A. Kammoun, and M. S. Alouini, "Performance of multibeam very high throughput satellite systems based on feeder links with nonlinearity," *IEEE Trans. Wireless Commun.*, vol. 19, no. 9, pp. 5908–5923, Jun. 2020.
[31] H. G. Sandalidis, T. A. Tsiftsis, and G. K. Karagiannidis, "Optical wireless communications with heterodyne detection over turbulence channels with pointing errors," *J. Lightw. Technol.*, vol. 27, no. 20, pp. 4440–4445, Oct. 2009.
[32] M. Patzold, U. Killat, and F. Laue, "An extended suzuki model for land mobile satellite channels and its statistical properties," *IEEE Trans. Veh. Technol.*, vol. 47, no. 2, pp. 617–630, May 1998.
[33] L. C. Andrews, R. L. Phillips, and C. Y. Hopen, *Laser Beam Scintillation With Applications*. Bellingham, WA, USA: SPIE Press, 1st ed., 2001.
[34] A. Jurado-Navas, A. Garcia-Zambrana, and A. Puerta-Notario, "Efficient lognormal channel model for turbulent communications," *IET Electron. Lett.*, vol. 43, no. 3, pp. 178–179, Feb. 2007.
[35] A. Papoulis and U. Pillai, *Probability, Random Variables and Stochastic Processes*. Boston, MA, USA: McGraw-Hill, 4th ed., 2002.
[36] I. Gradshteyn and I. Ryzhik, *Table of Integrals, Series, and Products*. Amsterdam, The Netherlands: Elsevier, 7th ed., 2007.
[37] Wolfram Research, Inc., Mathematica, Version 8.0, Champaign, Illinois, 2010.